In-plane elasticity of a novel auxetic honeycomb design

Jian Huang[a,c], Qiuhua Zhang[a], Fabrizio Scarpa[b,*], Yanju Liu[a], Jinsong Leng[c,*]

[a] *Department of Aerospace Science and Mechanics, No. 92 West Dazhi Street, Harbin Institute of Technology (HIT), P.O. Box 301, Harbin 150080, PR China*

[b] *Advanced Composites Center for Innovation and Science, University of Bristol, Bristol BS8 1TR, UK*

[c] *Center for Composite Materials and Structures, No. 2 Yikuang Street, Science Park of Harbin Institute of Technology (HIT), P.O. Box 301, Harbin, PR China*

Abstract: This work presents a novel negative Poisson's ratio honeycomb design composed by two parts (a re-entrant hexagonal component and a thin plate part) that provide separate contributions to the in-plane and out-of-plane mechanical properties. The re-entrant hexagons provide the in-plane negative Poisson's ratio, the in-plane compliance and the out-of-plane compressive strength, while the thin plate part connecting the re-entrant hexagonal section bears the large out-of-plane flexibility. This paper focuses on the in-plane mechanical properties of the auxetic cellular structure. Theoretical models related to the in-plane uniaxial tensile modulus, the shear modulus, and the Poisson's ratios have been built and validated using the finite element techniques. The in-plane behavior of the honeycomb has also been investigated against the geometrical parameters of the unit cell using a parametrical analysis. The theoretical and numerical models illustrate good agreement and show the potential of its application in morphing structures. We also provide a benchmark of the auxetic configuration proposed in this work against negative Poisson's ratio topologies from open literature.

Keywords: negative Poisson's ratio; honeycomb; cellular structure; auxetic.

1. Introduction

Due to the significant lightweight and designable in-plane and out-of-plane mechanical performances honeycomb structures have attracted worldwide attention for several decades [1, 2]. The primary application of honeycomb structures is to be used as sandwich core materials in various engineering fields, such as aerospace, marine and automotive lightweight structures [3, 4]. In recent years, honeycombs have also been proposed as a promising solution for the morphing skin [5-8]. Different honeycomb configurations result in different values of the in-plane Poisson's ratio. A variety of honeycomb configurations achieving positive/negative/zero Poisson's ratio have been proposed and investigated with special focus on the in-plane mechanics, flatwise compressive strength and the transverse shear modulus [9-25]. Honeycombs with negative Poisson's ratio (NPR) can likewise be described as auxetic [26-28]. When subject to out-of-plane bending deformation honeycombs with positive Poisson's ratio (PPR) show anticlastic or saddle-shape curvature that somehow limits their application in sandwich structures with complex out-of-plane geometry [4, 29, 30]. No lateral deformations can be observed when honeycombs exhibiting zero Poisson's ratio are loaded along one in-plane direction making them more suitable for one-dimensional

* Corresponding author
E-mail address: lengjs@hit.edu.cn (Jinsong Leng); f.scarpa@bristol.ac.uk (Fabrizio Scarpa).

(span) morphing[6, 31]. NPR honeycomb structures feature synclastic curvature behavior, therefore making possible to provide dome-shaped surfaces when loaded with out-of-plane bending deformation [30, 32]. Auxetic honeycombs have been employed to prototype radomes [33], adaptive and deployable structures [34], and morphing wings [35-37].

A ZPR cellular configuration made by combinations of hexagons and thin plates has been previously proposed by the authors to achieve large out-of-plane deformation abilities and separate tailorable design of the in-plane and out-of-plane performances [38, 39]. In-plane mechanics and the bending property of the ZPR cellular structure have been investigated. A comparison of the out-of-plane bending behavior of six different types of cellular configurations with the same relative density using the 3-point bending tests show that inserting the thin plate can achieve an enhanced bending compliance[39]. In this work, a similar honeycomb design exhibiting in-plane negative Poisson's ratio for large out-of-plane deformations and morphing applications is proposed and investigated. A re-entrant hexagonal structure and a thin plate are consisted in the honeycomb configuration. The re-entrant hexagonal section is designed to bear the out-of-plane compression and to produce in-plane negative Poisson's ratio and flexibility, while the thin plate is inserted for the large out-of-plane compliance. As a result, different sections bring about different mechanical properties leading to a separate design for the in-plane and out-of-plane performances. Analytical models to describe the in-plane elasticity of the novel honeycomb have been developed and validated using the Finite Element (FE) homogenization approaches. The dependence of the in-plane properties on the honeycomb geometrical parameters has also been further investigated using a combination of analytical models and FE homogenizations.

2. Geometry of the novel auxetic honeycomb design

The layout of the novel negative Poisson's ratio honeycomb structures and geometry of its unit cell are presented in Fig. 1. It's evident that the unit cell possesses a vertical and horizontal symmetry. The unit cell can be described by a re-entrant hexagonal structure and two thin plates connecting the re-entrant hexagonal sections. The lengths of the inclined wall and two vertical walls are represented by parameters l, $h=\alpha l$ and $h_1=\mu l$, respectively. The internal cell angle is represented by the parameter θ. The parameter $t=\beta l$ represents the thickness of the re-entrant hexagonal section. The dimensions of the thin plate are demonstrated by the length $l_1=\eta l$, the width $h=\alpha l$ and the thickness $b_1=\lambda l$. The thickness of the whole unit cell is represented by the parameter $b=\gamma l$. It should be noted that, to avoid the overlapping of cell walls the geometric constraints $\begin{matrix}\mu > \sin\theta \\ \alpha > (\beta(2+\sin\theta)+2\sin\theta\cos\theta)/\cos\theta\end{matrix}$ must be satisfied. In addition, the relative density of the novel auxetic honeycomb can be calculated by inspection as:

$$\frac{\rho}{\rho_c}=\frac{2\alpha\eta\lambda l^2+\gamma l^2[\alpha(\beta+2\cos\theta)-2\sin\theta\cos\theta+2\beta(\mu-\sin\theta)]-2c_1\gamma\cos\theta(a_1-c_1\sin\theta)]}{\gamma l^2(2\eta+2\cos\theta+\beta)(\alpha+2\mu-2\sin\theta)} \quad (1)$$

In (1) $a_1 = \alpha l - 2\beta l \cot(\frac{\pi}{4} - \frac{\theta}{2})$ and $c_1 = l - \beta l / (2\cos\theta)$ are respectively the length of the inner side of the vertical and the inclined walls of the unit cell.

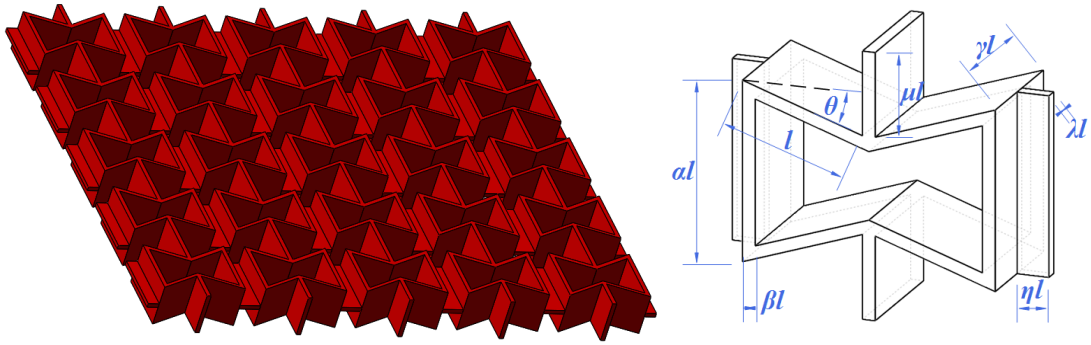

Fig.1. Geometry of the novel auxetic honeycomb structures

3. Theoretical models

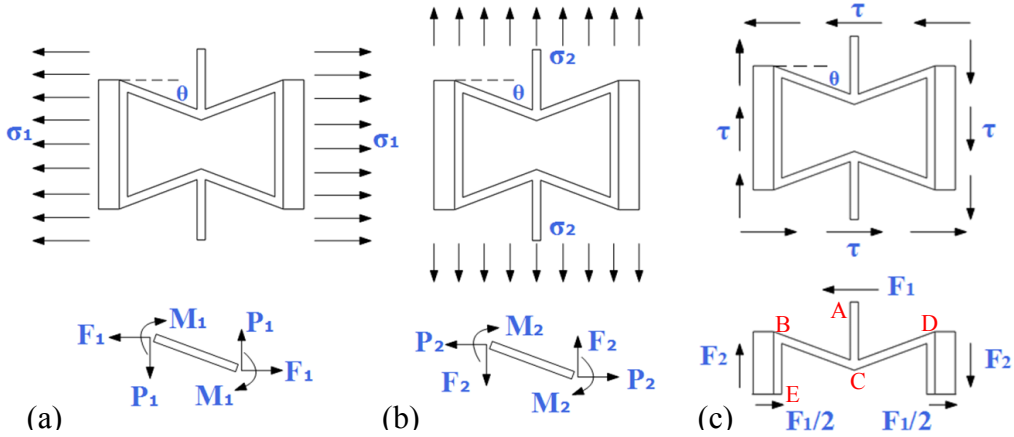

Fig. 2. Top view of unit cell models to calculate the theoretical in-plane mechanical constants: (a) tensile modulus along the 1 (horizontal) direction; (b) tensile modulus along the 2 (vertical) direction; (c) the in-plane shear modulus.

The analytical models to calculate the in-plane tensile modulus of the novel auxetic honeycomb structure developed in this paper are based on the application of the Castigliano's second theorem[40]. The honeycomb ribs are assumed to undergo bending and axial tensile deformation. The elastic modulus along the 1 (horizontal) direction of the honeycomb is calculated following the loading scheme shown in Fig.2 (a). The inclined walls are bent and stretched by the applied uniformly distributed stress σ_1 which is parallel to the 1 direction. It is evident that $P_1=0$, $F_1=\sigma_1 b(h-2l\sin\theta+2\mu l)/2$ and the bending moment M_1 can be obtained from the equilibrium equations [1]:

$$M_1 = \frac{1}{2} F_1 l \sin\theta \tag{2}$$

In this work, the positive bending moment is orientated along the anti-clockwise direction . The bending moment distribution and the axial tensile force on the single rib are:

$$M_1(x) = (\frac{1}{2}l - x)F_1 \sin\theta, F_{N1}(x) = F_1 \cos\theta \tag{3}$$

According to the Castigliano's second theorem, one obtains the strain energy of the single bending and stretched wall:

$$U_1 = \frac{F_1^2 l^3 \sin^2\theta}{24 E_s I} + \frac{F_1^2 l \cos^2\theta}{2 E_s A} \tag{4}$$

In (4), E_s is the Young's modulus of the honeycomb material, $I=\beta^3\gamma l^4/12$ and $A=\beta\gamma l^2$ the second moment of area and the area of the cross section of the inclined wall respectively. Using the Castigliano's second theorem herein, it is possible to calculate the horizontal deformation of the inclined wall:

$$\delta_{11} = \frac{F_1 l^3 \sin^2\theta}{12 E_s I} + \frac{F_1 l \cos^2\theta}{E_s A} \tag{5}$$

In order to take the thin plate into account, the axial tensile deformation induced by the applied stress σ_1 can be calculated as:

$$\delta_{12} = \frac{2F_1\eta}{E_s \alpha\lambda l} \tag{6}$$

The total deformation of the unit cell along the 1 (horizontal) direction can be therefore obtained as:

$$\delta_1 = 2(\delta_{11} + \delta_{12}) \tag{7}$$

With equation (7) and the geometry of the unit cell shown in Fig.1, one can obtain the homogenized strain along the horizontal direction:

$$\varepsilon_1 = \frac{\delta_1}{2(\eta l + l\cos\theta) + \beta l} \tag{8}$$

The homogenized and non-dimensional Young's modulus along the 1 direction can therefore be obtained from the ratio between the tensile stress σ_1 and strain ε_1:

$$\frac{E_1}{E_s} = \frac{\alpha\lambda\beta^3(\eta + \cos\theta + \frac{\beta}{2})}{(\frac{1}{2}\alpha + \mu - \sin\theta)[\alpha\lambda(\sin^2\theta + \beta^2\cos^2\theta) + 2\eta\gamma\beta^3]} \tag{9}$$

Following the same procedure, one can also obtain the homogenized and non-dimensional Young's modulus along the 2 direction. The loading scheme to calculate E_2/E_s is shown in Fig. 2(b). A uniformly distributed stress σ_2 has been applied on the unit cell along the 2 (vertical direction). It is also evident that $P_2=0$, $F_2=\sigma_2\gamma l(2\eta l+2l\cos\theta+\beta l)/2$ and from the equilibrium equations the bending moment can be calculated as:

$$M_2 = \frac{1}{2} F_2 l \sin\theta \tag{10}$$

The bending moment and the tensile force distribution along the inclined wall are given by:

$$M_2(x) = (\frac{1}{2}l - x)F_2\cos\theta,\ F_{N2}(x) = F_2\sin\theta \tag{11}$$

Again following the Castigliano's second theorem, one can obtain the strain energy and deformation along the 2 (vertical) direction of the bent and stretched inclined wall:

$$U_2 = \frac{F_2^2 l^3 \cos^2\theta}{24 E_s I} + \frac{F_2^2 l \sin^2\theta}{2 E_s A} \tag{12}$$

$$\delta_{21} = \frac{F_2 l^3 \cos^2\theta}{12 E_s I} + \frac{F_2 l \sin^2\theta}{E_s A} \tag{13}$$

In order to determine the dependence of the tensile modulus along the 2 direction on the geometric parameters of the central vertical wall, the axial tensile deformation of the central vertical wall has been taken into account herein:

$$\delta_{22} = \frac{2F_2\mu}{E_s\beta\gamma l} \tag{14}$$

Thus, one obtains the total deformation and strain of the unit cell induced by the applied uniformly distributed stress along the 2 direction as shown in Fig. 2(b),

$$\delta_2 = 2(\delta_{21} + \delta_{22}) \tag{15}$$

$$\varepsilon_2 = \frac{\delta_2}{\alpha l + 2\mu l - 2l\sin\theta} \tag{16}$$

The homogenized nondimensional Young's modulus along the 2 direction can also therefore be obtained from the ratio between the tensile stress σ_2 and strain ε_2:

$$\frac{E_2}{E_s} = \frac{\beta^3(\frac{\alpha}{2} + \mu - \sin\theta)}{(\eta + \cos\theta + \frac{\beta}{2})(2\mu\beta^2 + \beta^2 + \cos^2\theta - \beta^2\cos^2\theta)} \tag{17}$$

The Poisson's ratio of the novel auxetic honeycomb can be calculated by the definition of taking the negative ratio of the strain normal to over the strain parallel to the loading direction. When loading in the 1 (horizontal) direction, one can obtain the Poisson ratio as:

$$\nu_{12} = -\frac{\cos\theta(\eta + \cos\theta + \frac{\beta}{2})}{\sin\theta(\frac{\alpha}{2} + \mu - \sin\theta)} \tag{18}$$

And for loading in the 2 (vertical) direction:

$$\nu_{21} = -\frac{\sin\theta(\frac{\alpha}{2} + \mu - \sin\theta)}{\cos\theta(\eta + \cos\theta + \frac{\beta}{2})} \tag{19}$$

The loading scheme used to perform the theoretical calculation of the in-plane shear modulus of the novel auxetic honeycomb is shown in Fig. 2(c). A uniformly distributed shear stress has been applied on the unit cell, and because of the vertical symmetry a half model of the unit cell is used in the following calculation as shown in the bottom figure of Fig. 2(c). Due to the horizontal symmetry of the half model, there is no relative displacement among the points B, C, D, leading to that the shear deformation of the half model simplified into the sum of the horizontal deformations of the honeycomb struts AC and BE induced by applying the shear stress. In this work, the bending deformation of AC and BE, as well as the shear deformation of BE have been taken into account. It's evident that the relationship between the force F_1 and the applied stress τ can be described as:

$$F_1 = \tau\gamma l(2\eta l + 2l\cos\theta + \beta l) \tag{20}$$

The horizontal displacement of the point A against the point C can be obtain using the standard equation of the Euler-Bernoulli beam theory [40].

$$\delta_{121} = \frac{\tau\gamma\mu^3 l^5 (2\eta + 2\cos\theta + \beta)}{3E_s I} \tag{21}$$

The inclined wall and the central vertical wall have a same cross section, so the second moment of area of the cross section of the wall AC is also marked as *I*. In order to calculate the horizontal deformation of the honeycomb strut BE, the flexural center of this T-beam must be found. The geometry of the cross section of the T-beam is shown in Fig. 3. According Table 8.12 in the reference [40], one can find the distance between the flexural center and the origin of coordinates.

$$e = \frac{1}{2}(\beta l + \eta l)\frac{(\lambda l)^3 \eta l}{(\lambda l)^3 \eta l + (\gamma l)^3 \beta l} \tag{22}$$

For a thin-walled I-beam the central web carries the great majority of the shear stresses, and that is also apporiate for a thin-walled T-beam. In this paper only the shear deformation of the central web (the red dashed rectangle in Fig. 3) of the T-beam has been taken into account. According to the Timoshenko beam theory, the horizontal deformation of the strut BE which is a cantilever beam with a concentrated force loading at the free end can be calculated by:

$$\delta_{122} = \frac{F_1(\alpha l)^3}{48E_s I_1} + \frac{F_1 \alpha l}{4KA_1 G_s} \tag{23}$$

In equation (23), $G_s=E_s/(2+2\nu_s)$ is the shear modulus of the honeycomb material, ν_s the Poisson's ratio of the honeycomb material, *K* the Timoshenko shear coefficient of the red dashed rectangle in Fig. 3, I_1 and A_1, the second moment of area and the area of the cross section of the T-beam respectively. Evidently, $A_1=(\eta+\beta)\lambda l^2$ and the coefficient *K* [41] and the the second moment of area I_1 can be calculated following:

$$K = \frac{10(1+\nu_s)}{12+11\nu_s} \tag{24}$$

$$\begin{aligned} I_1 = {} & \frac{\gamma l^4}{24}\left[\left(\frac{\lambda^3\eta(\eta+\beta)}{\lambda^3\eta+\gamma^3\beta}+\beta\right)^3 - \left(\frac{\lambda^3\eta(\eta+\beta)}{\lambda^3\eta+\gamma^3\beta}-\beta\right)^3\right] \\ & + \frac{\lambda l^4}{24}\left[\left(2\eta+\beta-\frac{\lambda^3\eta(\eta+\beta)}{\lambda^3\eta+\gamma^3\beta}\right)^3 - \left(\beta-\frac{\lambda^3\eta(\eta+\beta)}{\lambda^3\eta+\gamma^3\beta}\right)^3\right] \end{aligned} \tag{25}$$

The shear strain of the half model of the unit cell is given by:

$$\gamma_{12} = \frac{\delta_{121}+\delta_{122}}{\frac{\alpha l}{2}+\mu l - l\sin\theta} \tag{26}$$

Using G=τ/γ, one can obtain the homogenized and nondimensional shear modulus of the novel auxetic honeycomb structure as:

$$\frac{G_{12}}{E_s} = \frac{\frac{\alpha}{2}+\mu-\sin\theta}{\gamma(2\eta l + 2l\cos\theta + \beta l)\left[\frac{(\mu l)^3}{3I}+\frac{(\alpha l)^3}{48I_1}+\frac{\alpha l(1+\nu_s)}{2KA_1}\right]} \tag{27}$$

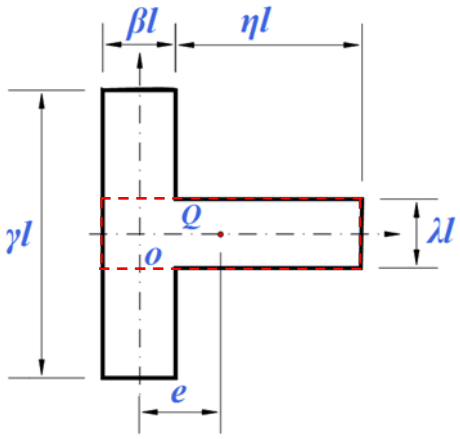

Fig.3. Geometry of the T-beam

4. Finite element homogenization

In order to validate the analytical models of the in-plane elasticity, the commercial finite element software ANSYS (version 13.0, ANSYS Inc.) was used to perform the numerical homogenization of the novel auxetic honeycomb structures. The models were developed using 3D structral elements (Solid 45) defined by 8 nodes and three translational degrees at each node. The full-size representative volumes were given by 5 ×5 unit cells (Fig. 4) with boundary conditions following [38, 42, 43]. According to the convergence tests, a minimum element size of $t/2$ was used in the simulations. The boundary conditions used to get the in-plane constants of the novel auxetic honeycomb were listed in Table 1. To obtain the tensile Young's modulus E_1 and the Poisson's ratio v_{12} the in-plane tension along the 1 direction was simulated with boundary conditions that the surfaces A and B were loaded with displacement conditions $u_1=\varepsilon_0*x_1$, $u_2= u_3=0$ where ε_0 was the tensile axial strain and x_1 the coordinate of the element nodes on the 1 direction, the surfaces C, D, E and F were set as free boundary conditions. The in-plane tension along the 2 direction was also simulated to get the tensile Young's modulus E_2 using similar boundary conditions with the simulated tension on the 1 direction as shown in Table 1. Displacements of $u_2=\varepsilon_0*x_2$, $u_1= u_3=0$ were loaded on the the surfaces C and D, where ε_0 was also the tensile axial strain and x_2 the coordinate of the element nodes on the 2 direction. Free boundary conditions were also applied on the surfaces A, B, E and F. In the case of the in-plane shear simulation, following [44] a cantilever beam clamp was used to apply the boundary conditions. Surface C was loaded with displacements equal to $u_1=\gamma_0*L_2$, $u_2=u_3=0$ where γ_0 was the shear strain, and L_2 the total length of the representative volumes along the 2 direction, and surface D was set as a fixed end. Mimicking a continuous honeycomb along the 1-direction surfaces A and B were subjected to anti-symmetrical boundary conditions. On surfaces E and F free boundary conditions were also applied. The average tensile stress and strain were calculated within the central unit cell (red ellipse in Fig. 4) [44] to avoid the Saint-Venant effect from the borders. The following equations were employed to calculate the average tensile and shear stresses [10]:

$$\bar{\sigma}_{ii} = \frac{1}{V}\int_V \sigma_{ii}(1,2,3)dV\,,\ \bar{\tau}_{12} = \frac{1}{V}\int_V \tau_{12}dV \tag{28}$$

The relations of stress and strain for a general orthogonal anisotropic material can be expressed as:

$$\begin{Bmatrix} \bar{\varepsilon}_1 \\ \bar{\varepsilon}_2 \\ \bar{\varepsilon}_3 \\ \bar{\gamma}_{23} \\ \bar{\gamma}_{13} \\ \bar{\gamma}_{12} \end{Bmatrix} = \begin{bmatrix} S_{11} & S_{12} & S_{13} & 0 & 0 & 0 \\ S_{21} & S_{22} & S_{23} & 0 & 0 & 0 \\ S_{31} & S_{32} & S_{33} & 0 & 0 & 0 \\ 0 & 0 & 0 & S_{44} & 0 & 0 \\ 0 & 0 & 0 & 0 & S_{55} & 0 \\ 0 & 0 & 0 & 0 & 0 & S_{66} \end{bmatrix} \begin{Bmatrix} \bar{\sigma}_1 \\ \bar{\sigma}_2 \\ \bar{\sigma}_3 \\ \bar{\tau}_{23} \\ \bar{\tau}_{13} \\ \bar{\tau}_{12} \end{Bmatrix} \tag{29}$$

Thus the in-plane compliance of the novel auxetic honeycomb were given by:

$$E_1 = 1/S_{11},\ E_2 = 1/S_{22},\ \nu_{12} = -S_{21}/S_{11},\ G_{12} = 1/S_{66} \tag{30}$$

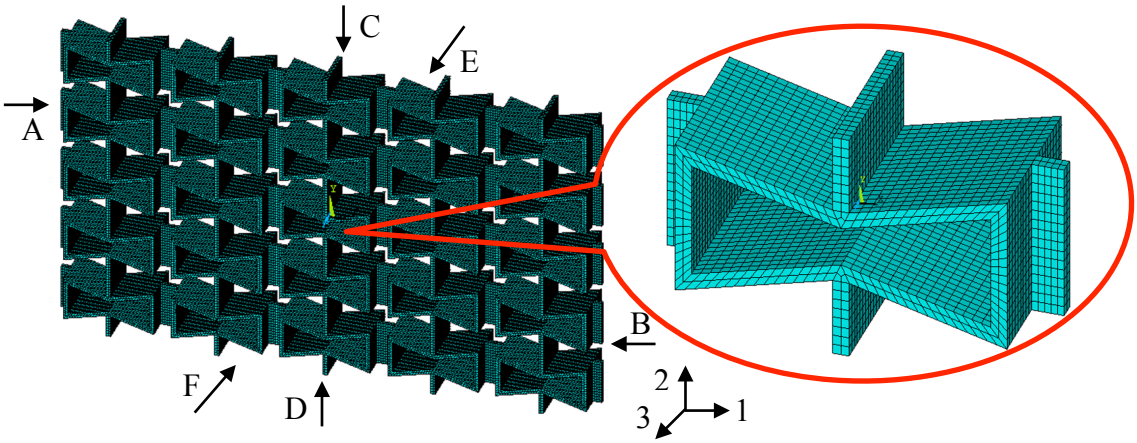

Fig.4. FE models used in the numerical simulations

Table 1 Boundary conditions used in the numerical simulations

Properties	Surfaces A and B	Surface C	Surface D	Surfaces E and F
E_1 and ν_{12}	$u_1=\varepsilon_0*x_1$ $u_2=0$ $u_3=0$	Free	Free	Free
E_2	Free	$u_1=0$ $u_2=\varepsilon_0*x_2$ $u_3=0$		Free
G_{12}	anti-symmetry	$u_1=\gamma_0*L_2$ $u_2=0$ $u_3=0$	Fixed	Free

5. Results and discussions

5.1. The in-plane tensile modulus

For all the calculations in this paper the length of the inclined wall has been set as 10mm and isotropic properties of E_s=1.6GPa, ν_s=0.3 have been used for the honeycomb material. The existing of the re-entrant hexagonal section in the novel auxetic honeycomb leads to a similar in-plane tensile stiffness with the one described by the Gibson and Ashby model for the classical centersymmetric hexagonal configuration[1].Fig. 5 and 6 demonstrate the FE homogenization and analytical predictions of the non-dimensional in-plane elastic modulus E_1/E_s versus the cell angles

for various parameters α and β. In general, the non-dimensional elastic modulus E_1/E_s decreases with increasing cell angles θ while the other geometrical parameters keep constant. As shown in both figures, the results of the FE simulations and the analytical models show generally good agreements with each other when the cell angle is larger than 10°, while large discrepancies occur if θ≤10°. For example, as shown in Fig. 5 the analytical results is averagely 51.17% stiffer than the FE homgenizations when θ≤10° for α=2.0, but that data for the case of θ>10° reduces to 8.64%. Apparently, neglecting the shear deformation in the analytical model results in a slightly stiffer tensile modulus of the novel auxetic honeycomb than the analogous one from the FE simulation when θ>10°. And when θ≤10° the shear deformation contributes substantially to the whole honeycomb deformation that leads to a relatively larger discrepancy between the analytical and FE results. Increasing of the parameter α will decrease the nondimentional tensile modulus of the novel auxetic honeycomb along the 1-direction while other geometrical parameters keep constant. On the opposite, the nondimensional tensile modulus on the 1-direction increases substantially while the parameter β increases, for instance the in-plane tensile modulus shows an averagely increase of more than 2600% when the parameter β varies from 0.05 to 0.15. It provides a good way to design the in-plane tensile modulus by varying parameter β. Fig. 7 and 8 show the values of the nondimensional modulus E_1/E_s from FE homogenizations versus the cell angles at different γ and μ values. Decreases are observed on these two figures when the values of γ and μ increse keeping the rest parameters constant.

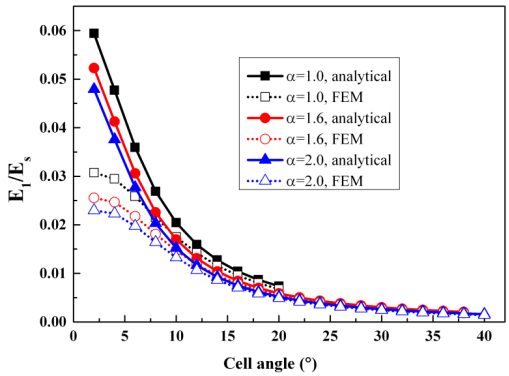

Fig. 5. FE homogenization and analytical predictions of the non-dimensional in-plane elastic modulus E_1/E_s versus the cell angles for various parameters α while β=0.1, η=0.1, γ=1.0, λ=0.1, μ=1.0;

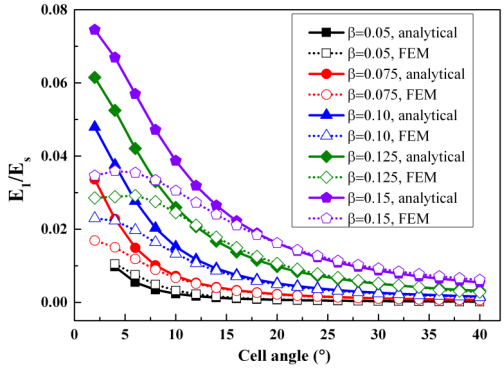

Fig. 6. FE homogenization and analytical predictions of the non-dimensional in-plane elastic modulus E_1/E_s versus the cell angles for various parameters β while α=2.0, η=0.1, γ=1.0, λ=0.1, μ=1.0;

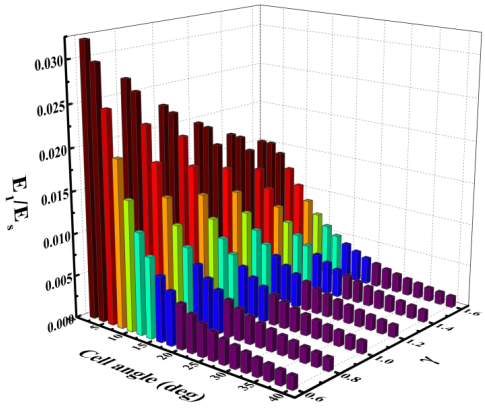

Fig. 7. FE homogenization of the non-dimensional in-plane elastic modulus E_1/E_s versus the cell angles for various parameters γ while α=2.0, β=0.1, η=0.1, λ=0.1, μ=1.0;

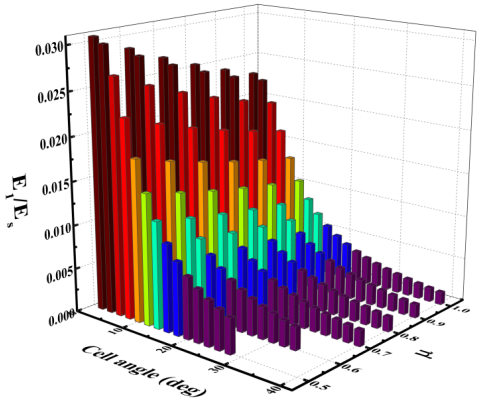

Fig. 8. FE homogenization of the non-dimensional in-plane elastic modulus E_1/E_s versus the cell angles for various parameters μ while α=2.0, β=0.1, η=0.1, λ=0.1,γ=1.0;

Figs. 9-12 demonstrate the variation of the non-dimensional in-plane tensile modulus on the 2-direction (E_2/E_s) versus cell angles for different geometrical parameters of the

unit cell. The analytical equation shows a very close comparison with the trends followed by the results of the FE homogenization. Neglecting the deformation of the T-beam and the shear deformation of the inclined wall results in a slightly stiffer analytical tensile modulus than the datas obtained through the FE homogenizations. For example, the analytical results is averagely 10.30% stiffer than the results from FE simulations when the parameter α equal to 2.0. Generally, the non-dimensional tensile modulus decreses slightly and then increase clearly when the cell angle varies from 2° to 40°. From Fig. 9 one can draw the conclusion that increasing of the parameter α leads to an increase of the in-plane tensile modulus. Fig. 10 shows a significant increase of the non-dimensional tensile modulus when the parameter β increases. An increse of the more than 1200% of the non-dimensional tensile modulus show up when the parameter β varies from 0.05 to 0.125 which makes varing β also a good design method for E_2/E_s. Figs. 11 and 12 illustrate the analytical predictions of the non-dimensional in-plane elastic modulus E_2/E_s versus the cell angles for various parameters η and μ. An increase of the parameter η leads to a decrease of the non-dimensional tensile modulus. Conversely, an increase of the parameter μ results in an increase of the same mechanical property.

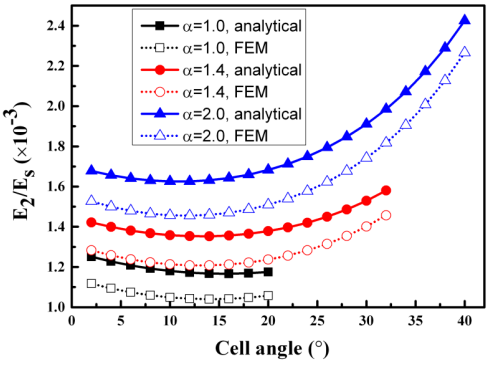

Fig. 9. FE homogenization and analytical predictions of the non-dimensional in-plane elastic modulus E_2/E_s versus the cell angles for various parameters α while β=0.1, η=0.1, γ=1.0, λ=0.1, μ=1.0;

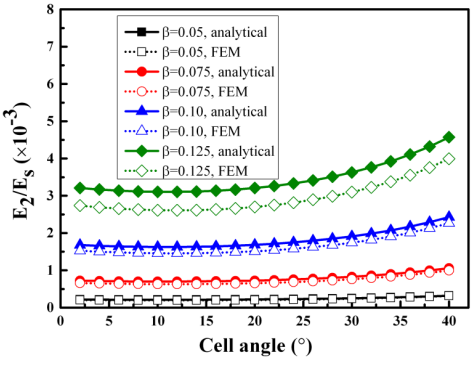

Fig.10. FE homogenization and analytical predictions of the non-dimensional in-plane elastic modulus E_2/E_s versus the cell angles for various parameters β while α=2.0, η=0.1, γ=1.0, λ=0.1, μ=1.0;

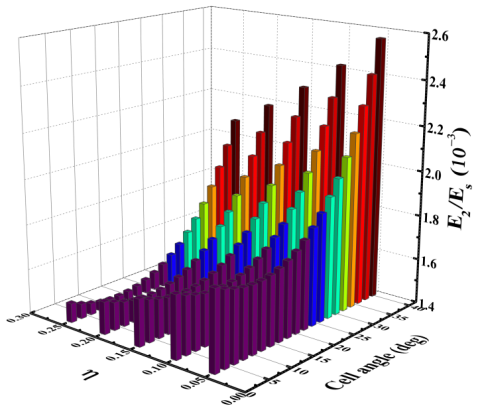

Fig.11. Analytical predictions of the non-dimensional in-plane elastic modulus E_2/E_s versus the cell angles for various parameters η while α=2.0, β=0.1, γ=1.0, λ=0.1, μ=1.0;

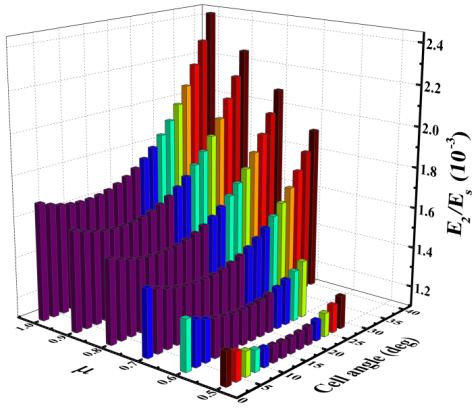

Fig.12. Analytical predictions of the non-dimensional in-plane elastic modulus E_2/E_s versus the cell angles for various parameters μ while α=2.0,β=0.1, η=0.1, γ=1.0, λ=0.1;

5.2. Poisson's ratio

Figs. 13-16 show the variation of the in-plane Poisson's ratio v_{12} of the novel auxetic honeycomb versus cell angles for different geometrical parameters. It must be pointed out that the existing of the re-entrant hexagonal section in the novel auxetic honeycomb structure produces a similar in-plane Poisson's ratio that also prodicts infinite values in the vicinity of an internal cell angle of 0° as the one described by Gibson and Assby [1]. But when the cell angle is relatively large (larger than 15°)the analytical results show good agreements with the analogous datas from the FE homogenization. To make it clear, the analytical Poisson's ratio is only 3.80% over the one predicted by the FE homogenization when θ=30° and α=1.4, β=0.1, η=0.1, γ=1.0, λ=0.1, μ=1.0. The FE homogenization of the in-plane Poisson's ratio versus cell angles for different geometrical parameters have been illustrated in Figs 13-16. Apparently, the Poisson's ratio reduces quickly to 0 when the cell angle is less than a certain degree (10° in Fig. 13), increases slowly when the cell angle is larger than the certain degree leading to a smallest value of the Poisson ratio at that value of the cell angle. The increasing of the cell wall aspect ratio α leads to an increasing of the Poisson's ratio. And the Poisson's ratio also increases when the parameter β increases. Moreover, the increasing of the parameter β would also lead to an increase of the certain value that dividing the trends of the Poisson's ratio against the cell angles. The certain degree of the cell angle

increases from 8° to 14° when the parameter varies from 0.05 to 0.15. Fig.15 show the FE homogenization of the Poisson's ratio v_{12} versus the cell angles for various parameters η while α=2.0, β=0.1, γ=1.0, λ=0.1, μ=1.0. An increase of the parameter η leads to a slightly increase of the Poisson's ratio when the cell angle is less than the certain degree, but the Poisson's ratio shows an opposite trend when the cell angle is larger than the certain degree. Fig. 16 shows the values of the Poisson's ratio from FE homogenizations versus cell angles at different μ values and constant α=2.0, β=0.1, η=0.1, γ=1.0, λ=0.1. The Poisson's ratio show clearly increases when the geometrical parameter μ varies from 0.5 to 1.0.

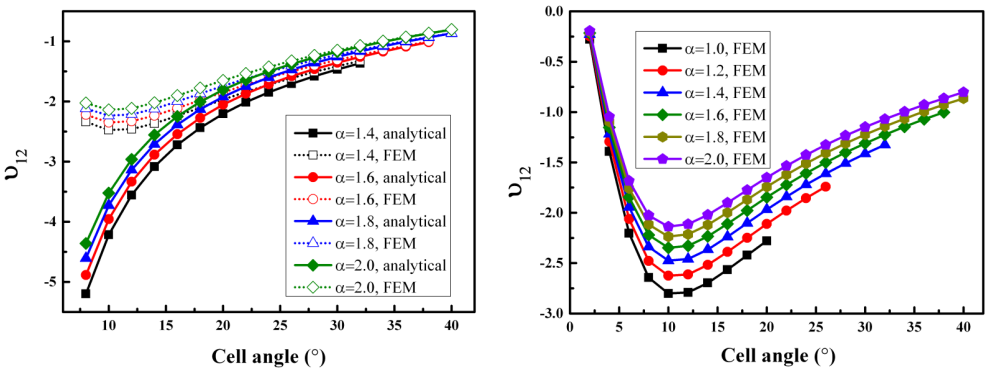

Fig.13. FE homogenization and analytical predictions of the Poisson's ratio v_{12} versus the cell angles for various parameters α while β=0.1, η=0.1, γ=1.0, λ=0.1, μ=1.0;

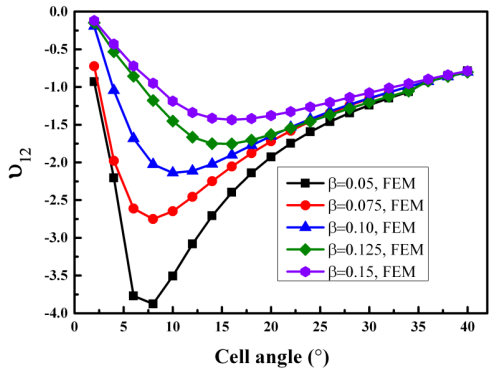

Fig.14. FE homogenization of the Poisson's ratio v_{12} versus the cell angles for various parameters β while α=2.0, η=0.1, γ=1.0, λ=0.1, μ=1.0;

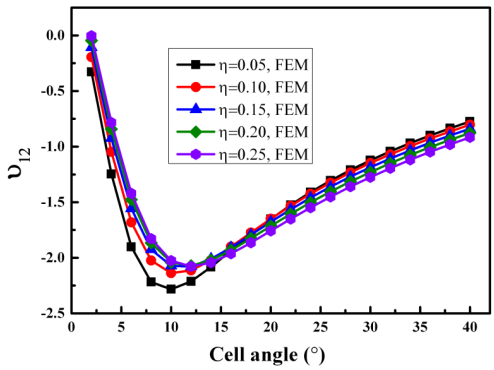

Fig.15. FE homogenization of the Poisson's ratio v_{12} versus the cell angles for various

parameters η while α=2.0, β=0.1, γ=1.0, λ=0.1, μ=1.0;

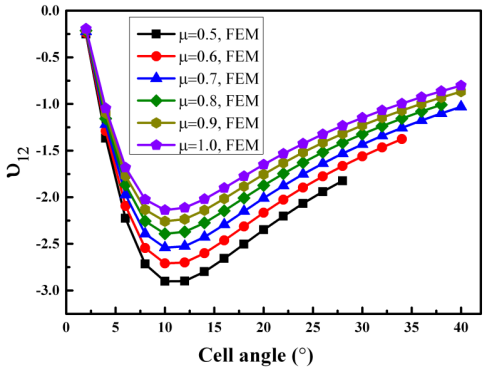

Fig.16. FE homogenization of the Poisson's ratio v_{12} versus the cell angles for various parameters μ while α=2.0, β=0.1, η=0.1, γ=1.0, λ=0.1;

5.3. in-plane shear modulus

Generally, there are three major boundary conditions (uniaxial, biaxial and tangential loading [45]) can be used to simulate a pure in-plane shear deformation. In this work, the tangential loading has been used in the FE homogenizations, and the analytical equation of the in-plane shear modulus is obtained using a pure shear model. Even the fixture of the tangential loading provide a pure shear deformation as closely as the ideal one, there are still some differences between a real pure in-plane shear deformation and an approximate one[44]. In the procedure of the calculation of the in-plane shear modulus, assumming that the web of the thin-walled T-beam bears all the shear stress and neglecting the shear stress in the flanges of the T-beam also produces some difference between the analytical and FE results. However, the analytical results show good agreements with the analogous ones from the FE homogenizations. A maximum discrepancy of only 2.60% has been observed between the two results when the cell angle θ varies from 0° to 38° for α=1.6, β=0.1, η=0.1, γ=1.0, λ=0.1, μ=1.0. Figs. 17-18 show the variation of the non-dimensional in-plane shear modulus against the internal cell angles for different geometrical parameters α and β of the unit cell. The non-simensional in-plane shear modulus decreases when the cell angle increases. On the contrary, an increase of cell wall aspect ratios α and β leads to also an increase of the non-simensional in-plane shear modulus. It must be noted that even a small increase of the parameter β can lead to a large increase of the non-dimensional in-plane elastic modulus providing that varying β is a good way for the design of the in-plane shear modulus. From Fig. 18, the discrepancy between the analytical and FE results also increases when the parameter β increases. That's because the shear deformation of the central vertical wall has been neglected in the analytical model and taken into account in the FE homogenizations. Increasing of the parameter β leads an increase of the ratio of the shear deformation of the central vertical wall over the whole deformation of the unit cell. Figs. 19-21 demonstrate the analytical predictions of the non-dimensional in-plane elastic modulus G_{12}/E_s versus the cell angles for various parameters γ, λ, μ respectively while the other parameters keep constant. Evidently, an increase of the three parameters all lead to the increasing of the non-dimensional in-plane elastic modulus.

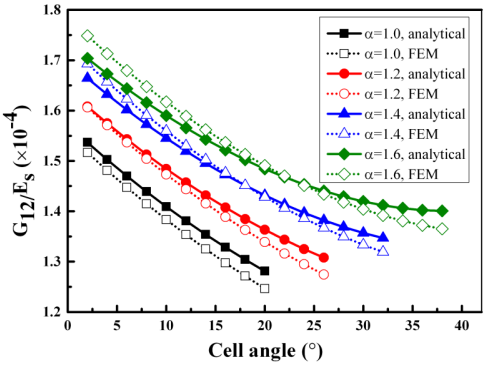

Fig.17. FE homogenization and analytical predictions of the non-dimensional in-plane elastic modulus G_{12}/E_s versus the cell angles for various parameters α while β=0.1, η=0.1, γ=1.0, λ=0.1, μ=1.0;

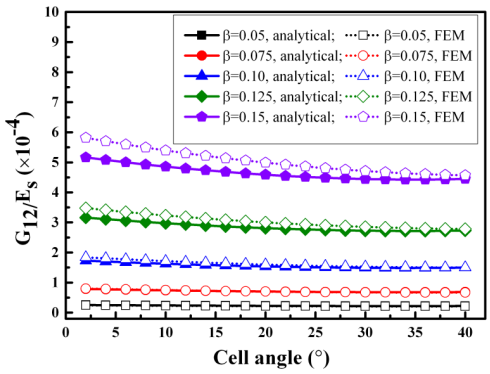

Fig.18. FE homogenization and analytical predictions of the non-dimensional in-plane elastic modulus G_{12}/E_s versus the cell angles for various parameters β while α=2.0, η=0.1, γ=1.0, λ=0.1, μ=1.0;

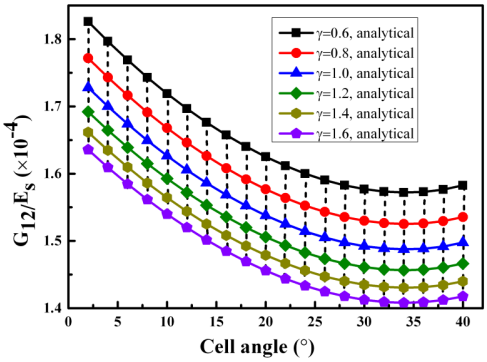

Fig.19. Analytical predictions of the non-dimensional in-plane elastic modulus G_{12}/E_s versus the cell angles for various parameters γ while α=2.0, β=0.1,η=0.1, λ=0.1, μ=1.0;

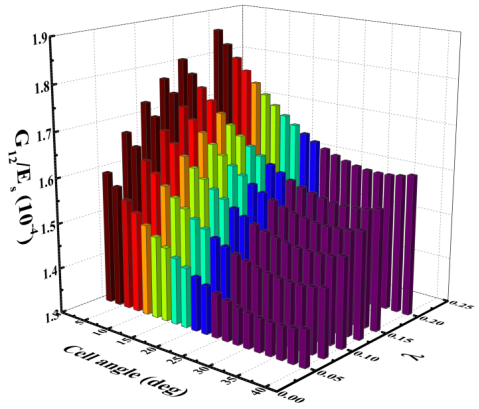

Fig.20. Analytical predictions of the non-dimensional in-plane elastic modulus G_{12}/E_s versus the cell angles for various parameters λ while α=2.0, β=0.1,η=0.1, γ=1.0, μ=1.0;

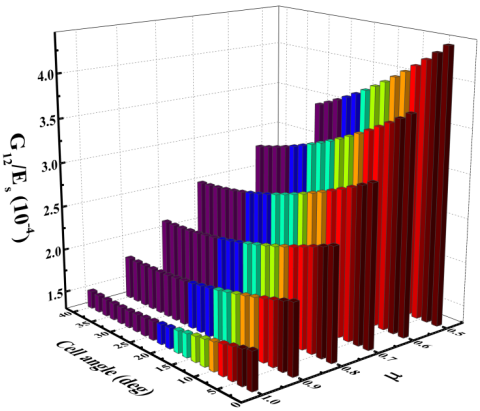

Fig.21. Analytical predictions of the non-dimensional in-plane elastic modulus G_{12}/E_s versus the cell angles for various parameters μ while α=2.0, β=0.1,η=0.1, γ=1.0, λ=0.1;

5.4. Comparison with existing auxetic configurations

A benchmark of the in-plane mechanics of the cellular configuration against three different auxetic cellular structures is shown in Fig. 1. The results for the re-entrant hexagonal configurations have been calculated using the typical formulas contained in [1], for internal cell angles ranging from -40° to -10° and cell wall aspect ratios equal to 1.0, 1.2, 1.4, 1.6, 1.8, 2.0. The choice of these angles stems from avoiding the extremely large anisotropy along the 1-direction when the internal cell angle is near to zero, The data representing the anti-tetra-chiral are obtained using equations sourced from [46], for cell wall aspect ratio r/L varying from 0.05 to 0.45 and a constant cell wall thickness ratio t/L of 0.1. The results of the novel auxetic configuration have also been calculated with internal cell angles ranging from -40° to -10°, and cell wall aspect ratios of 1.0, 1.2, 1.4, 1.6, 1.8, 2.0 while the other parameters keep constants. The novel auxetic honeycomb presented in this work shows very similar results to the classical re-entrant hexagonal configuration for the tensile modulus along the 1-direction, the Poisson's ratio and the in-plane shear modulus. The tensile modulus along the 2-direction of the re-entrant configuration however varies between 3.27 and 17.20, while the novel auxetic structure tends to cluster in a relative small interval (7.20-12.51). The same can be also stated for the in-plane Poisson's ratios and modulus along the 1-direction, with most of the results belonging to the new configuration being clustered in a nondimensional

density interval $\rho/\rho_c/\beta$ between 1.05 and 1.7. Note that the dimensionless Young's modulus along the 2-direction of the anti-tetrachiral honeycomb is equal to the one along the 1-direction because of isotropy. The insertion of thin plate parts in the novel configuration appears to provide a smaller relative density when compared with the one of the re-entrant hexagonal honeycomb. The anti-tetra-chiral honeycomb generally provides a much higher relative density when compared with the other two cellular configurations. The in-plane Poisson's ratio of the anti-tetra-chiral honeycomb is also very close to -1, even when the relative density increases. One of the biggest features of the new cellular configuration is the high specific shear stiffness at very low dimensionless densities (below 1.4), as well as the negative in-plane Poisson's ratio higher (in terms of magnitude) than the one provided by the classical re-entrant of butterfly shape at $\rho/\rho_c/\beta$ lower than 1.25.

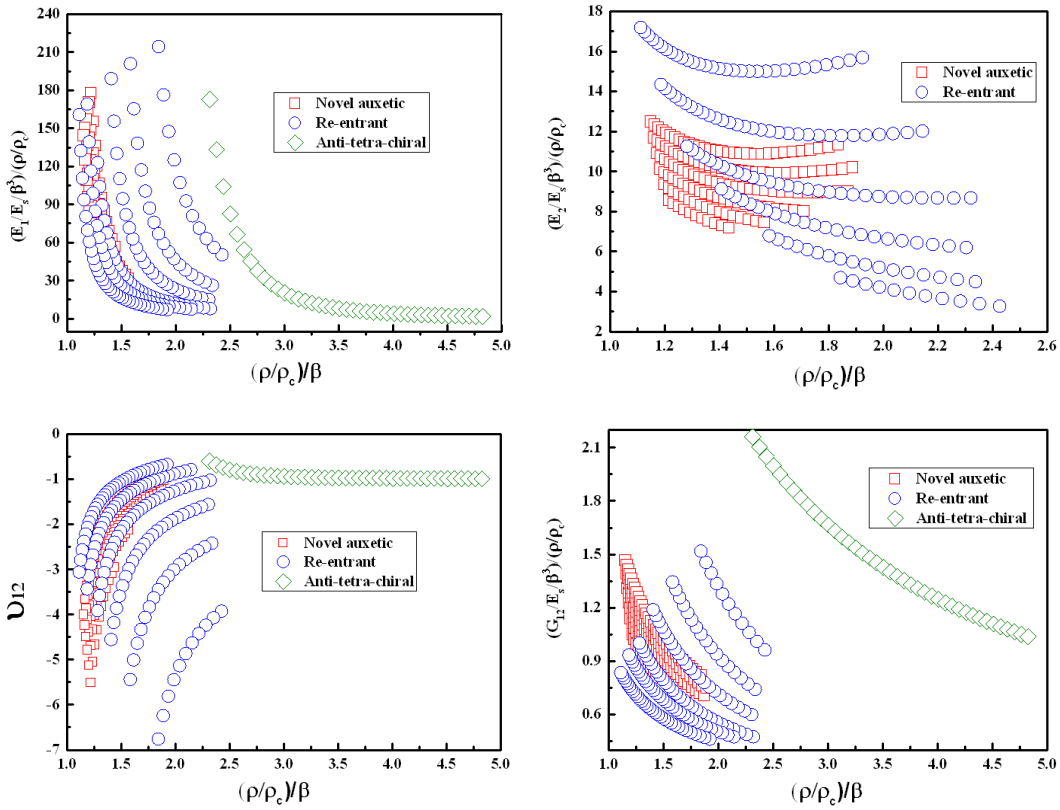

Fig. 22. Comparison of the in-plane elasticity between the novel auxetic honeycomb, the classical re-entrant configuration and the anti-tetra-chiral topologies.

6. Conclusions

In this work a novel auxetic honeycomb structure for large out-of-plane deformations and morphing structures has been proposed and the novelty of the auxetic honeycomb topology assembles two geometrical entities together: the re-entrant hexagonal structures to provide the out-of-plane compressive strength and to produce in-plane negative Poisson's ratio and compliance, and a thin plate that inserted for the large out-of-plane flexibility. The two entities bring about different contributions to the homogenized mechanical properties leading to a separate design for the in-plane and out-of-plane performances. The analytical models for the in-plane tension modulus

along both the two directions, the in-plane Poisson's ratio and the in-plane shear modulus have been developed and validated by FE homogenizations. The parametric analyses show that it is possible to obtain large variations and control of the design of the in-plane mechanics through the variation of the unit cell geometric parameters making this novel auxetic honeycomb structure particularly interesting for morphing structures.

Acknowledgements
The support of the FP7-AAT.2012.6.3-1-341509 MORPHELLE and the National Natural Science Foundation of China (Grant No.11225211) are gratefully acknowledged.

References

[1] Gibson LJ, Ashby MF. Cellular solids: structure and properties: Cambridge university press; 1997.

[2] Bitzer T. Honeycomb technology: materials, design, manufacturing, applications and testing: Springer Science & Business Media; 1997.

[3] Alderson A, Alderson K, Attard D, Evans K, Gatt R, Grima J, et al. Elastic constants of 3-, 4-and 6-connected chiral and anti-chiral honeycombs subject to uniaxial in-plane loading. Composites Science and Technology. 2010;70(7):1042-8.

[4] Alderson A, Alderson K, Chirima G, Ravirala N, Zied K. The in-plane linear elastic constants and out-of-plane bending of 3-coordinated ligament and cylinder-ligament honeycombs. Composites Science and Technology. 2010;70(7):1034-41.

[5] Olympio K, Gandhi F. Zero-v Cellular Honeycomb Flexible Skins for One-Dimensional Wing Morphing. 2007.

[6] Olympio KR, Gandhi F. Zero-Nu Cellular Honeycomb Flexible Skins for One-Dimensional Wing Morphing. 48th Structures, Structural Dynamics, and Materials Conference2007. p. 23-6.

[7] Olympio KR, Gandhi F. Flexible skins for morphing aircraft using cellular honeycomb cores. Journal of intelligent material systems and structures. 2009.

[8] Bubert EA, Woods BK, Lee K, Kothera CS, Wereley NM. Design and fabrication of a passive 1D morphing aircraft skin. Journal of Intelligent Material Systems and Structures. 2010;21(17):1699-717.

[9] Scarpa F, Tomlin P. On the transverse shear modulus of negative Poisson's ratio honeycomb structures. Fatigue & Fracture of Engineering Materials & Structures. 2000;23(8):717-20.

[10] Sun C, Vaidya R. Prediction of composite properties from a representative volume element. Composites Science and Technology. 1996;56(2):171-9.

[11] Lira C, Scarpa F. Transverse shear stiffness of thickness gradient honeycombs. Composites Science and Technology. 2010;70(6):930-6.

[12] Liu L, Wang H, Guan Z. Experimental and numerical study on the mechanical response of Nomex honeycomb core under transverse loading. Composite Structures. 2015;121:304-14.

[13] Lorato A, Innocenti P, Scarpa F, Alderson A, Alderson K, Zied K, et al. The transverse elastic properties of chiral honeycombs. Composites Science and Technology. 2010;70(7):1057-63.

[14] Scarpa F, Panayiotou P, Tomlinson G. Numerical and experimental uniaxial loading on in-plane auxetic honeycombs. The Journal of Strain Analysis for Engineering Design. 2000;35(5):383-8.

[15] Bezazi A, Scarpa F, Remillat C. A novel centresymmetric honeycomb composite structure.

Composite Structures. 2005;71(3-4):356-64.
[16] Grima JN, Gatt R, Alderson A, Evans K. On the potential of connected stars as auxetic systems. Molecular Simulation. 2005;31(13):925-35.
[17] Prall D, Lakes R. Properties of a chiral honeycomb with a Poisson's ratio of—1. International Journal of Mechanical Sciences. 1997;39(3):305-14.
[18] Miller W, Smith C, Scarpa F, Evans K. Flatwise buckling optimization of hexachiral and tetrachiral honeycombs. Composites Science and Technology. 2010;70(7):1049-56.
[19] Chen Y, Scarpa F, Liu Y, Leng J. Elasticity of anti-tetrachiral anisotropic lattices. International Journal of Solids and Structures. 2013;50(6):996-1004.
[20] Lira C, Scarpa F, Olszewska M, Celuch M. The SILICOMB cellular structure: Mechanical and dielectric properties. physica status solidi (b). 2009;246(9):2055-62.
[21] Chen DH. Bending deformation of honeycomb consisting of regular hexagonal cells. Composite Structures. 2011;93(2):736-46.
[22] Chen DH. Equivalent flexural and torsional rigidity of hexagonal honeycomb. Composite Structures. 2011;93(7):1910-7.
[23] Gong X, Huang J, Scarpa F, Liu Y, Leng J. Zero Poisson's ratio cellular structure for two-dimensional morphing applications. Composite Structures. 2015;134:384-92.
[24] Lira C, Scarpa F, Tai Y, Yates J. Transverse shear modulus of SILICOMB cellular structures. Composites Science and Technology. 2011;71(9):1236-41.
[25] Neville R, Monti A, Hazra K, Scarpa F, Remillat C, Farrow I. Transverse stiffness and strength of Kirigami zero-ν PEEK honeycombs. Composite Structures. 2014;114:30-40.
[26] Evans KE, Nkansah MA, Hutchinson IJ, Rogers SC. Molecular Network Design. Nature. 1991;353(6340):124-.
[27] Lim T-C. Auxetic Materials and Structures: Springer; 2015.
[28] Poźniak AA, Wojciechowski KW, Grima JN, Mizzi L. Planar auxeticity from elliptic inclusions. Composites Part B: Engineering. 2016;94:379-88.
[29] Evans K. The design of doubly curved sandwich panels with honeycomb cores. Composite Structures. 1991;17(2):95-111.
[30] Lakes R. Foam structures with a negative Poisson's ratio. Science. 1987;235(4792):1038-40.
[31] Olympio KR, Gandhi F. Zero Poisson's ratio cellular honeycombs for flex skins undergoing one-dimensional morphing. Journal of intelligent material systems and structures. 2010;21(17):1737-53.
[32] Evans K, Alderson K. Auxetic materials: the positive side of being negative. Engineering Science and Education Journal. 2000;9(4):148-54.
[33] Scarpa F, Smith FC, Chambers B, Burriesci G. Mechanical and electromagnetic behaviour of auxetic honeycomb structures. Aeronaut J. 2003;107(1069):175-83.
[34] Hassan MR, Scarpa F, Ruzzene M, Mohammed NA. Smart shape memory alloy chiral honeycomb. Mater Sci Eng A-Struct Mater Prop Microstruct Process. 2008;481:654-7.
[35] Spadoni A, Ruzzene M, Scarpa F. Global and local linear buckling behavior of a chiral cellular structure. Phys Status Solidi B-Basic Solid State Phys. 2005;242(3):695-709.
[36] Martin J, Heyder-Bruckner JJ, Remillat C, Scarpa F, Potter K, Ruzzene M. The hexachiral prismatic wingbox concept. Phys Status Solidi B-Basic Solid State Phys. 2008;245(3):570-7.
[37] Bettini P, Airoldi A, Sala G, Di Landro L, Ruzzene M, Spadoni A. Composite chiral structures

for morphing airfoils: Numerical analyses and development of a manufacturing process. Compos Pt B-Eng. 2010;41(2):133-47.
[38] Huang J, Gong X, Zhang Q, Scarpa F, Liu Y, Leng J. In-plane mechanics of a novel zero Poisson's ratio honeycomb core. Composites Part B: Engineering. 2016;89:67-76.
[39] Huang J, Zhang Q, Scarpa F, Liu Y, Leng J. Bending and benchmark of zero Poisson's ratio cellular structures. Composite Structures. 2016;152:729-36.
[40] Young WC, Budynas RG. Roark's formulas for stress and strain: McGraw-Hill New York; 2002.
[41] Cowper GR. The Shear Coefficient in Timoshenko's Beam Theory. Journal of Applied Mechanics. 1966;33(2):335-40.
[42] Odegard GM. Constitutive modeling of piezoelectric polymer composites. Acta materialia. 2004;52(18):5315-30.
[43] Chen YJ, Scarpa F, Liu YJ, Leng JS. Elasticity of anti-tetrachiral anisotropic lattices. International Journal of Solids and Structures. 2013;50(6):996-1004.
[44] Singer J, Arbocz J, Weller T. Buckling Experiments: Experimental Methods in Buckling of Thin-walled Structures. Shells, Built-up Structures, Composites and Additional Topics: John Wiley & Sons; 2002.
[45] Salit V, Weller T. On the feasibility of introducing auxetic behavior into thin-walled structures. Acta Materialia. 2009;57(1):125-35.
[46] Mousanezhad D, Haghpanah B, Ghosh R, Hamouda AM, Nayeb-Hashemi H, Vaziri A. Elastic properties of chiral, anti-chiral, and hierarchical honeycombs: A simple energy-based approach. Theoretical and Applied Mechanics Letters. 2016;6(2):81-96.